RSC Advances

PAPER

View Article Online
View Journal | View Issue

Cite this: *RSC Adv.*, 2015, **5**, 48928

A rechargeable sodium-ion battery using a nanostructured Sb–C anode and P2-type layered $Na_{0.6}Ni_{0.22}Fe_{0.11}Mn_{0.66}O_2$ cathode

Ivana Hasa,[a] Stefano Passerini*[bc] and Jusef Hassoun*[a]

Received 9th April 2015
Accepted 26th May 2015

DOI: 10.1039/c5ra06336a

www.rsc.org/advances

Herein we report the realization and characterization of a full sodium-ion cell using a P2-$Na_{0.6}Ni_{0.22}Fe_{0.11}Mn_{0.66}O_2$ layered oxide positive electrode (cathode) and a nanostructured Sb–C alloying negative electrode (anode). X-Ray Diffraction (XRD), Scanning Electron Microscopy (SEM) and transmission electron microscopy (TEM) reveal the well-defined layered-structure of the cathode and the presence of nanometric antimony trapped within the carbon matrix of the anode. The optimized materials structures allow enhanced performance of each electrode in cells with sodium metal anodes, as revealed by electrochemical characterization including cyclic voltammetry (CV) and galvanostatic cycling (GC), further improved by the addition of fluoroethylene carbonate (FEC) into the electrolyte. Finally, the performance of the rechargeable Sb–C/$Na_{0.6}Ni_{0.22}Fe_{0.11}Mn_{0.66}O_2$ sodium-ion battery using the FEC-added electrolyte solution is reported. Such a cell shows an average working voltage of about 2.7 V while delivering a stable capacity of about 120 mA h g^{-1}, leading to a theoretical energy density of about 300 W h kg^{-1}, based on the cathode weight. The expected practical energy of industrial cells based on this chemistry, calculated using the 1/3 reduction factor accounting for inactive components and packaging as derived from Li-ion batteries, is about 100 W h kg^{-1}, which is to be considered to be an extremely promising value.

1. Introduction

Recent global concerns have triggered the need for energy conversion and storage systems (ESSs) characterized by high efficiency and low cost in order to fulfil the demand of clean and renewable energy sources. Electrochemical energy storage systems, such as batteries and supercapacitors, play a crucial role in this field. Among these, lithium-ion batteries (LIBs) are one of the most common and diffused secondary batteries.[1,2] High energy density, efficiency and long life have so far allowed the success of LIBs, promoting their large diffusion in the portable electronic market and in the automotive field as the power source of choice.[3] However, concerns about the long-term availability of lithium sources and their restricted geographical localization are presently moving the focus on different technologies. Several attempts are presently devoted to the identification and the development of alternative, economically sustainable secondary batteries as complementary systems to the lithium-based one, such as room temperature Na-based energy storage systems.[4,5] In fact, sodium is, in principle, a promising candidate due to its high abundance, thus low cost, and geographic distribution, although it promises lower energy storage with respect to lithium due to the higher atomic weight and electrochemical potential.[6,7] Therefore, Na-ion batteries (NIBs) are considered a very suitable system for application in the stationary energy storage field, in which low cost and long cycle life are the most important characteristics. Efforts on the development of suitable electrodes and electrolyte solutions have led to promising materials for Na batteries.[8,9] Among the cathode materials, polyanionic compounds and transition metal, layered oxides reveal the best electrochemical performances. Indeed, phosphates based materials, such as $NaFePO_4$ and Na_2FePO_4F,[10,11] show good thermal stability and high operating voltage due to the inductive effect of the $(PO_4)^{3-}$ polyanion. Furthermore, layered oxide materials are characterized by high specific capacity and easy synthesis pathway. Sodium-based transition metal layered oxides have been largely investigated as reversible insertion materials for sodium-ion batteries. Single transition metal oxides, such as Na_xCoO_2 and Na_xMnO_2, evidenced low delivered capacity and poor capacity retention upon cycling.[12,13] Partial substitution of the sodium-based oxides by electrochemical active or inactive transition metals represented one of the most promising strategy, commonly adopted to improve the behavior of the layered cathode in sodium cells.[14,15] Indeed, the beneficial effect of the contemporary presence of various metals within the layered structure have led

[a]*Department of Chemistry, "Sapienza" University of Rome, Piazzale Aldo Moro, 5, 00185 Rome, Italy. E-mail: jusef.hassoun@uniroma1.it*

[b]*Helmholtz Institute Ulm, Helmholtzstraße 11, 89081 Ulm, Germany. E-mail: stefano.passerini@kit.edu*

[c]*Karlsruhe Institute of Technology (KIT), PO Box 3640, 76021 Karlsruhe, Germany*

to the development of binary or ternary transition metal oxides characterized by improved structural stability and remarkable cycling behavior. Among them, manganese and iron-based materials appeared of particular interest due to the high abundance and low cost. Indeed, our approach to cathode materials design was to introduce Fe and Ni to Mn-based layered compounds. The introduction of nickel plays a crucial role in the achievement of high capacity values, since it contributes by double-electron process to the overall electrochemical insertion of sodium ions into the metal layers.[16,17]

Despite the development of several cathode materials, the identification of suitable negative electrodes still represents the challenge to face in order to achieve the effective application of Na-based battery. The use of metallic sodium represents a serious issue to overcome in order to increase the intrinsic safety of sodium-based cells.[18] Analogously to lithium, amorphous carbon, conversion and alloying materials are considered the most promising candidates as Na-ion anode materials.[19–21] Indeed, Sn, Sb and Ge may accommodate Na^+ ions according to the alloying mechanism:

$$M + xNa^+ + xe^- = Na_xM.$$

However, sodium alloying reaction leads to lower capacity in respect to lithium in view of the limited alloying-degree achieved during the process, due to the large ionic radius of sodium.[22] On the other hand, one advantage of sodium based materials respect to the lithium ones may be the higher value of the Na^+/Na potential compared to Li^+/Li, which is expected to reduce electrolyte degradation at the surface of the electrode material. This represents a relevant issue for alloying materials in which the electrode/electrolyte interface is continuously renewed upon cycling.[23]

Similarly to Li-alloy anode materials, the strain associated to the huge volume change occurring upon alloying and de-alloying, leads to the electrode material disintegration during cycling and consequent cell failure. Basing on lithium experience, trapping nanoparticles of active material within a carbon matrix represents the most suitable strategy to buffer the volume variation.[24,25]

Among the alloying materials, Sb-based composites revealed attracting electrochemical performances as anode alternative to metal sodium. Indeed, Sb is characterized by high theoretical capacity, of about 660 mA h g^{-1} and a relatively limited volume expansion with respect to other Na-alloying metals.[26–28]

In this work we characterized two electrode materials for application in sodium-ion battery, *i.e.* P2-$Na_{0.6}Ni_{0.22}Fe_{0.11}Mn_{0.66}O_2$ transition metal layer oxide cathode and nanostructured Sb–C alloying anode. These electrodes have been studied both in the electrolyte composed of $NaClO_4$, propylene carbonate (PC) and fluoroethylene carbonate (FEC) as additive.

As shown later, the optimized structural and morphological characteristics of the electrodes allow enhanced electrochemical behavior in sodium cell in terms of cycling stability and high delivered capacity. Combining the two electrodes and the FEC-added electrolyte results in a sodium-ion battery with an average working voltage of about 2.7 V and delivering a stable capacity of about 120 mA h per gram of active cathode material. We would point out that further improvement on the cell components, in particular the electrolyte, may lead to enhanced performances and safety content of the cell. Accordingly, this attractive low cost energy storage system is here proposed as a proof of concept, lab scale prototype suitable of further optimization, *e.g.* by using safe, perchlorate free electrolyte salt and proper combination of carbonate based solvents or even safer ionic liquid based electrolytes.

2. Results and discussion

2.1. The Sb–C electrode

Fig. 1 shows the structural and morphological characteristics of the nanostructured anode material as detected by X-ray diffraction (a), scanning electron microscopy (b) and transmission electron microscopy (c). The XRD pattern shows the peaks ascribed to the hexagonal Sb (JCPDS no. 35-0732) with no sign of impurities. Using the Scherrer equation ($D = K\lambda/B\cos\theta$), the Sb crystallite average size in the nanocomposite was calculated to be of about 34 nm, which is in good agreement with the SEM (Fig. 1(b)) and the TEM (Fig. 1(c)) micrographs, revealing Sb nanoparticles of a size lower than 50 nm uniformly dispersed within the carbon matrix. This particular morphology is expected to allow stable cycling behavior of the material in sodium cell, as indeed demonstrated in the following.

Cyclic voltammetry test was performed in order to check the sodium (de)-alloying electrochemical process. Fig. 2 reports the cyclic voltammogram of a three-electrode sodium cell using an Sb–C electrode as the working electrode and 1 M $NaClO_4$-PC as the electrolyte. During the first cathodic scan (sodiation process), the CV reveals a series of peaks at about 0.8 V and 0.45 V associated to two overlapping processes, *i.e.*, the solid electrolyte interface (SEI) formation and the Na–Sb alloying process, which are accompanied by the structural reorganization of the electrode/electrolyte interface.[26] The reversible peaks at very low voltage values, *i.e.*, at about 0.01 V in reduction and 0.02 V in oxidation, during the first (de)-sodiation process may be ascribed to the intercalation of sodium ions into the amorphous carbon matrix.[19] In the following cycles 3 reduction features, a single peak at about 0.7 V and a doublet at 0.45 V *vs.* Na/Na^+, are observed during the cathodic scan, which result into 2 oxidation peaks, at about 0.8 V and 0.9 V *vs.* Na/Na^+, during the subsequent anodic scan. The cathodic and anodic peaks are highlighted by dot-circles in the voltammogram in Fig. 2. These peaks reflect the reversible Na–Sb alloying process evolving trough a multi-step reaction, *i.e.*, initial formation of the amorphous Na_xSb phase followed by that of the hexagonal Na_3Sb.[29]

Galvanostatic cycling tests were performed on Na/Sb–C cells in order to check the suitability of the Sb–C nanocomposite material for battery application. Fig. 3 compares the performance of such cells using, as the electrolyte, the 1 M solution of $NaClO_4$ in PC (a) and PC : FEC (b). The voltage profile of the Na/Sb–C cell using the former electrolyte (see Fig. 3(a)) reveals two

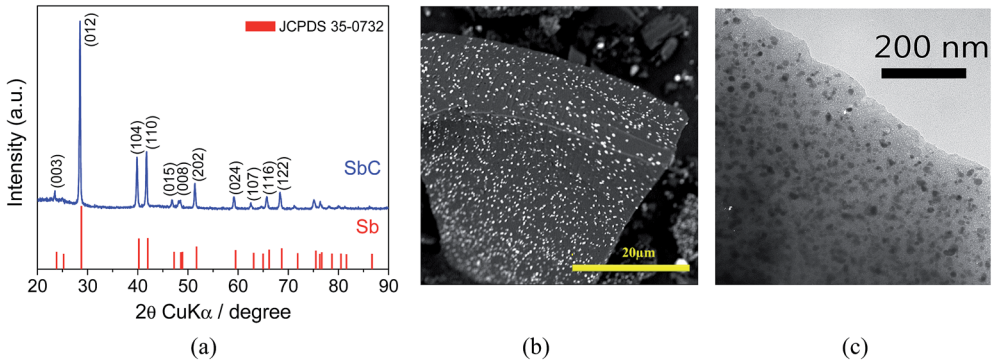

Fig. 1 (a) XRD pattern of the Sb–C nanocomposite and Sb reference pattern (JCPDS 35-0732). (b) SEM and (c) TEM images of the Sb–C nanocomposite.

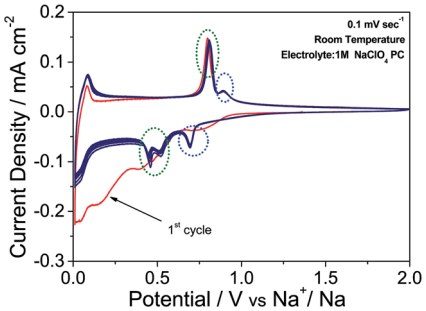

Fig. 2 Cyclic voltammetry (CV) profile of the Na/Sb–C cell. Test performed using a scan rate of 0.1 mV sec^{-1} within the 0.01–2.0 V *vs.* Na^+/Na potential range. Temperature: 25 °C. Electrolyte: 1 M $NaClO_4$ in PC.

plateaus at about 0.45 V and 0.7 V during the alloying process (discharge), shifting at about 0.8 V and 0.9 V during de-alloying (charge), in complete agreement with the redox processes observed upon CV tests (compare with Fig. 2). The alloying process at about 0.7 V becomes more clearly visible during the following cycles (see figure inset) as a result of the structural reorganization of the material upon the first discharge–charge (see above). The initial discharge capacity of the Sb–C electrode is about 450 mA h g^{-1}, while the subsequent charge capacity reaches a value of 203 mA h g^{-1}. However, this cell, using the 1 M solution of $NaClO_4$ in PC, shows a huge capacity fading by cycling, resulting in the low specific capacity (about 100 mA h g^{-1}) after 50 cycles. This capacity decay may be ascribed to a non-optimized SEI film formation in the conventional electrolyte.[23] A remarkable improvement of the Sb–C cycling stability is, however, achieved using the FEC-containing electrolyte, as demonstrated in Fig. 3(b). With such an electrolyte, a similar electrode behavior is observed during the first cycle (compare Fig. 3(a) and (b)), except for the presence of an additional irreversible voltage plateau at about 1.2 V. This latter is attributed to the reductive decomposition of the FEC added to the electrolyte solution, leading to the formation of a protective passivation layer at the electrode/electrolyte interface and consequent stabilization of the electrode behavior.[23] Indeed, the Na/Sb–C cell with FEC-added electrolyte delivers a capacity of about 375 mA h g^{-1} and 210 mA h g^{-1} during the first discharge and following charge, respectively, and stabilizes at about 200 mA h g^{-1} during the subsequent 50 charge–discharge cycles (see inset of Fig. 3(b)). The great improvement of the Sb–C cycling behavior and coulombic efficiency when using the FEC-added electrolyte is clearly demonstrated by the comparison reported in Fig. 3(c). The capacity retention upon 50 cycles approaches 50% for the cell using the electrolyte without FEC and about 90% for that using the FEC-added solution. Furthermore, the change of the electrolyte solution remarkably improves the Na/Sb–C cell coulombic efficiency, *i.e.* from a value approaching 90% with the bare electrolyte to values higher than 98% with the FEC-added one.

The performance of the Na/Sb–C cells using the FEC-added electrolyte was further investigated in terms of rate capability. Fig. 3(d) reports the charge–discharge profiles at various current densities, *i.e.* 10, 50 and 100 mA g^{-1}, during the 1st and, in inset, the 10th cycles. The Sb–C electrode cycled at 10 mA g^{-1} shows an initial discharge capacity of about 610 mA h g^{-1} and a following charge capacity of about 286 mA h g^{-1}. Increasing current values lead to discharge capacities of about 374 mA h g^{-1} (at 50 mA g^{-1}) and 219 mA h g^{-1} (at 100 mA g^{-1}) reversed into 210 mA h g^{-1} and 104 mA h g^{-1} during charge, respectively. Upon 10 charge–discharge cycles, the cells evidence a capacity retention of about 89%, 99% and 84% at 10, 50 and 100 mA g^{-1} current, respectively, with coulombic efficiency values of 86%, 95% and 96%. These data evidence that lower current rates lead to higher capacities as expected by decreased electrode polarization. However, slightly lower coulombic efficiency, due to a pronounced effect of side reactions, such as electrolyte decomposition, is also detected at lower rates thus suggesting intermediate current values (*i.e.* 50 mA g^{-1}) as preferred condition for long-term cycling tests.

2.2. The $Na_{0.6}Ni_{0.22}Fe_{0.11}Mn_{0.66}O_2$ electrode

Fig. 4 reports the structural and morphological characteristics of $Na_{0.6}Ni_{0.22}Fe_{0.11}Mn_{0.66}O_2$. The X-ray diffraction pattern reported in Fig. 4(a) reveals a layered structure belonging to the hexagonal *P*63/*mmc* space group, indexed as a P2-type structure

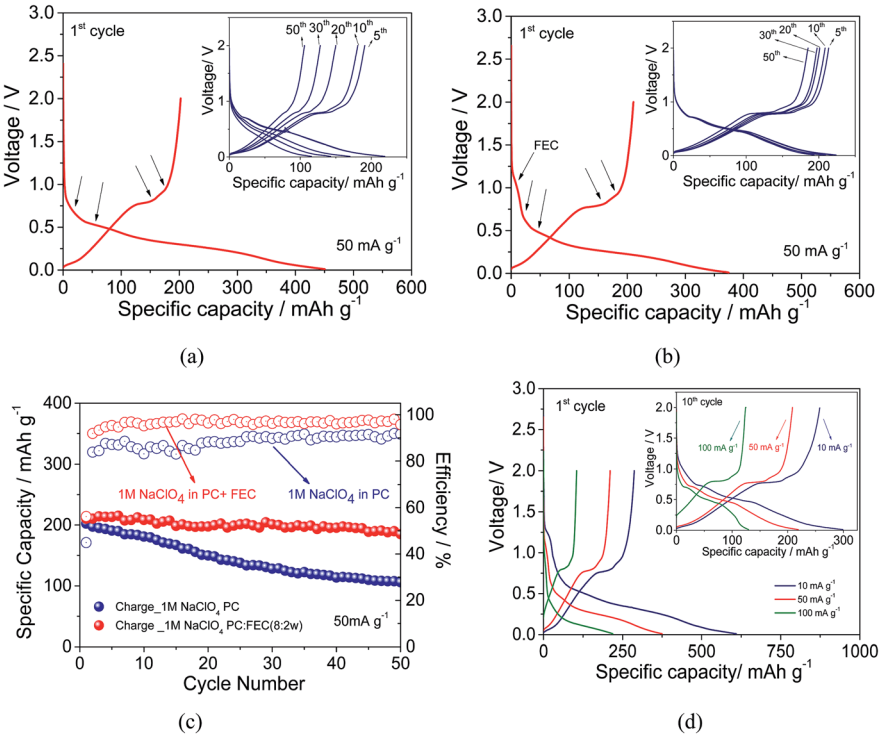

Fig. 3 Voltage profile of the first cycle and subsequent cycles (in insets) of the Na/Sb–C half-cells using 1 M $NaClO_4$ in PC (a) and 1 M $NaClO_4$ in PC : FEC, 8 : 2 w/w (b) electrolyte. Tests run at 50 mA g^{-1} within the 0.01–2.0 V voltage range at room temperature (25 °C). (c) Comparison of the cycling behavior and corresponding efficiency of the Na/Sb–C half-cells using 1 M $NaClO_4$ in PC (blue dots) and 1 M $NaClO_4$ in PC : FEC, 8 : 2 w/w (red dots) electrolyte. (d) Voltage profile of the first cycle and, in inset, of the tenth cycle of the Na/1 M $NaClO_4$ in PC : FEC, 8 : 2 w/w/Sb–C at different current rates: 10 mA g^{-1} (blue curves); 50 mA g^{-1} (red curves) and 100 mA g^{-1} (green curves).

with no signs of peaks attributable to impurities. Furthermore, the SEM image in Fig. 4(b) clearly shows the typical morphology of layered transition metal oxides, characterized by a sequence of planes forming single particles with an average size of about 1 to 2 μm. The P2-$Na_{0.6}Ni_{0.22}Fe_{0.11}Mn_{0.66}O_2$ electrode, already characterized in our previous work,[17] is here electrochemically studied using the FEC-added electrolyte solution for a later application in sodium-ion battery.

Fig. 5(a) compares the cycle performance, in terms of delivered capacity and coulombic efficiency, of the P2-$Na_{0.6}Ni_{0.22}Fe_{0.11}Mn_{0.66}O_2$ cathode in sodium half-cells using the conventional 1 M $NaClO_4$ in PC electrolyte and the FEC-added one. As seen in the figure, the use of FEC positively influences the electrochemical behavior of the cathode material both in

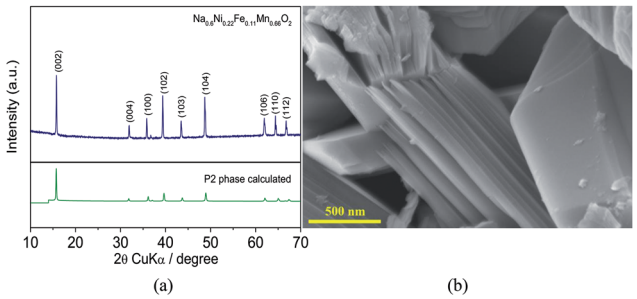

Fig. 4 X-ray diffraction pattern of the P2-$Na_{0.6}Ni_{0.22}Fe_{0.11}Mn_{0.66}O_2$ cathode material (a) and corresponding SEM images (b).

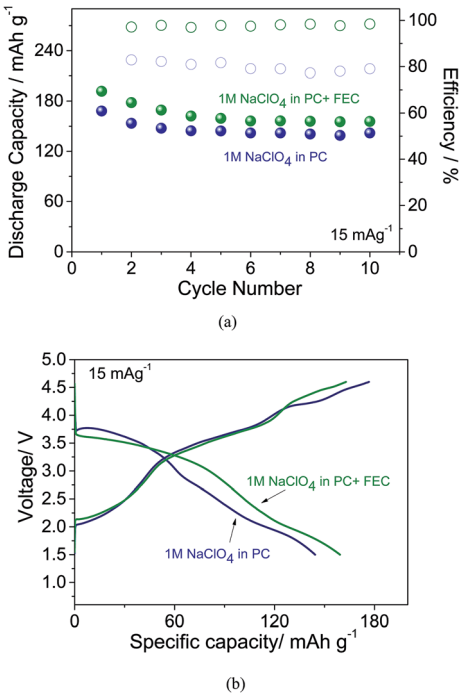

Fig. 5 (a) Galvanostatic cycling behavior and corresponding efficiency plot of the cell Na/P2-$Na_{0.6}Ni_{0.22}Fe_{0.11}Mn_{0.66}O_2$ half-cell using 1 M $NaClO_4$ in PC (blue dots) and 1 M $NaClO_4$ in PC : FEC, 8 : 2 w/w (green dots) electrolyte. (b) Voltage profiles of the two cells at the steady state condition (fifth cycle). Test performed at 15 mA g^{-1} at room temperature (25 °C) within 4.6–1.5 V voltage range.

terms of delivered capacity and of efficiency. The reversible capacity obtained using the conventional electrolyte is about 168 mA h g^{-1} during the first cycle and it decreases to about 142 mA h g^{-1} upon 10 cycles, with a capacity retention of about 84% and a coulombic efficiency approaching 80%. Instead, the cell using the FEC-added electrolyte shows higher capacity and improved coulombic efficiency. The first discharge capacity of the cell reaches 191 mA h g^{-1} with a capacity retention of about 82% upon 10 cycles and a coulombic efficiency enhanced up to 98%. These results clearly suggest an improved sodium (de)-insertion process, as indeed demonstrated by the comparison of the voltage profiles at the 5th cycle reported in Fig. 5(b).

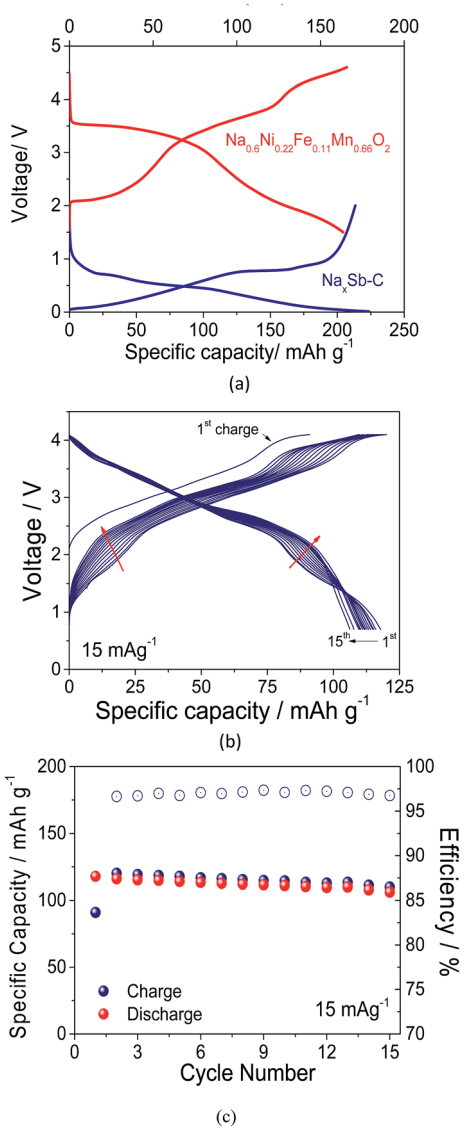

Fig. 6 (a) Comparison of the steady state voltage profiles of P2-$Na_{0.6}Ni_{0.22}Fe_{0.11}Mn_{0.66}O_2$ and Sb–C electrodes in sodium half-cell cycled at 30 mA g^{-1}. (b) Voltage profile of the Sb–C/1 M $NaClO_4$ PC : FEC, 8 : 2 w/w/$Na_{0.6}Ni_{0.22}Fe_{0.11}Mn_{0.66}O_2$ full cell cycled at room temperature (25 °C) at 15 mA g^{-1} and (c) corresponding cycling behavior and efficiency plots (c).

2.3. The Sb–C/$Na_{0.6}Ni_{0.22}Fe_{0.11}Mn_{0.66}O_2$ full cell

Taking into account the electrochemical characteristics of the Sb–C and $Na_{0.6}Ni_{0.22}Fe_{0.11}Mn_{0.66}O_2$ electrodes in sodium half-cell, which voltage *versus* capacity profiles are compared in Fig. 6(a), Sb–C/1 M $NaClO_4$ PC : FEC (8 : 2 w/w)/$Na_{0.6}Ni_{0.22}Fe_{0.11}Mn_{0.66}O_2$ full sodium-ion cell was assembled. This cell was cycled within the 4.1–0.7 V voltage range at a constant current of 15 mA g^{-1} (with respect to the cathode weight). Prior to full cell assembly, the Sb–C anode was electrochemically pre-activated by cycling in sodium metal half-cell. This pre-sodiation was performed to eliminate the initial irreversible capacity of the alloying anode and to partially sodiate it, thus compensating the Na-deficiency of the P2-type $Na_{0.6}Ni_{0.22}Fe_{0.11}Mn_{0.66}O_2$ cathode.[30] Considering the average working voltages of 3.2 V and 0.5 V for the layered oxide cathode and the Sb–C nanocomposite anode, respectively, it is reasonably assumed that the cell operates at about 2.7 V, as indeed demonstrated by Fig. 6(b) reporting the voltage profiles of the battery. The figure reveals a signature reflecting the (de-)alloying of Na with the Sb–C anode and its contemporary (de-)intercalation within the $Na_{0.6}Ni_{0.22}Fe_{0.11}Mn_{0.66}O_2$ layered structure. After an initial irreversible cycle, ascribed to the structural rearrangement of the layered cathode,[16] the cell assumes a stable behavior with reversible capacity around 120 mA h g^{-1} and coulombic efficiency approaching 97% (see Fig. 6(c)). Furthermore, the cell showes, upon cycling, decreasing polarization and, contemporary, modification of the voltage shape. These features reveal changes in the cell balance upon cycling, most likely attributed to side reactions at the electrode interphases. Considering the cell capacity and its working voltage (see Fig. 3(c)), the developed sodium-ion battery can provide a theoretical energy density of about 300 W h kg^{-1}.

3. Conclusion

P2-$Na_{0.6}Ni_{0.22}Fe_{0.11}Mn_{0.66}O_2$ layered oxide cathode and nanostructured Sb–C alloying anode were herein characterized as electrode materials for application in Na-ion batteries. The beneficial effect on both materials exerted by the addition of FEC into the electrolyte solution, improving the electrolyte/electrode interface, was proved. Rechargeable Sb–C/$Na_{0.6}Ni_{0.22}Fe_{0.11}Mn_{0.66}O_2$ sodium-ion battery showed average working voltage of about 2.7 V and delivered a reversible capacity of about 120 mA h g^{-1}. As a result, the adopted cell configuration allowed a theoretical energy density of about 300 W h kg^{-1}. Using the reduction factor of 1/3 to account for inactive components such as electrolyte separator, current collectors and cell case (as in Li-ion batteries), it is expected that industrially produced Sb–C/$Na_{0.6}Ni_{0.22}Fe_{0.11}Mn_{0.66}O_2$ Na-ion cells would deliver specific energy about 100 W h kg^{-1}. The satisfactory energy density and cycling performances suggest the Na-ion battery chemistry proposed herein as an attractive, low cost, energy storage system suitable for further optimization.

4. Experimental

4.1. Material synthesis and characterization

P2-type layered $Na_{0.6}Ni_{0.22}Fe_{0.11}Mn_{0.66}O_2$ (NFM) was prepared by a procedure recently developed in our laboratory,[16,17] consisting of solid–state reaction between sodium hydroxide (NaOH, Sigma Aldrich, >98%) and a nickel–iron–manganese precursor. The precursor was obtained by co-precipitation method dissolving stoichiometric proportions of $NiSO_4 \cdot 6H_2O$ (Sigma Aldrich, 99%), $FeSO_4 \cdot 7H_2O$ (AnalaR NORMAPUR, analytical reagent) and $MnSO_4 \cdot 5H_2O$ (AnalaR NORMAPUR, analytical reagent) in water and adding drop-wise an aqueous solution of NaOH (50% excess). After extensive rinsing with water, the obtained precursor was dried under vacuum. The powder precursor and NaOH were subsequently mixed in a molar ratio of 1 : 0.685. The mixture was annealed at 500 °C in air atmosphere and then as pellet at 900 °C. Finally the material was subjected to a water treatment. Inductively coupled plasma optical emission spectrometry (ARCOS ICP-OES, Spectro Analytical Instruments, Kleve, Germany) was used to determine the transition metal ratio and the sodium content in the sample. Structural and morphological characterization of the sample were detected respectively by X-Ray Diffraction (XRD, Rigaku Dmax Ultima + X-ray diffractometer) with CuKα radiation in the 2θ range from 10° to 90° and Field Emission Scanning Electron Microscopy analysis (FE-SEM, Zeiss Auriga).

The Sb–C nanostructured composite was prepared following a procedure originally developed in our laboratory for lithium-ion battery anodes.[31,32] The Sb–C composite material synthesis consisted of the infiltration of an organometallic antimony precursor, triphenylantimony(III) (Aldrich, 99%), in an organic resorcinol (benzene-1,3-diol)-formaldehyde (methanol) gel. The obtained gel was aged overnight and subsequently subjected to a washing process firstly with water and then with *tert*-butanol (Aldrich, 99%+). The impregnation step involved the immersion of the gel in a solution of triphenylantimony(III) (Aldrich, 99%), toluene (Aldrich, puriss.) and *tert*-butanol, in a mass ratio of 1 : 1 : 4. The recovered red gel was calcined at 700 °C for 3 h under argon flux. The Sb–C structure was investigated by XRD, using a D-max Ultima + Rigaku X-ray diffractometer using a CuKα radiation in the 2θ range from 20° to 90°. The sample morphology was investigated by scanning electron microscopy using a Phenom-FEI instrument and by transmission electron microscopy using a JEOL instrument. According to electrochemical measurements performed in conventional lithium cells,[31] the Sb content within the nanostructured Sb–C electrode is evaluated to be of the order of 30%. The nominal capacity of the electrode material is about 280 mA h g^{-1} with the carbon contribution accounting for 100 mA h g^{-1}.

4.2. Electrochemical characterization

$Na_{0.6}Ni_{0.22}Fe_{0.11}Mn_{0.66}O_2$ and Sb–C electrodes were prepared by dispersing the active material (80% w/w), carbon black super P (Timcal, 10% w/w) and polyvinylidene fluoride (PVdF 6020, Solvay, 10% w/w) in an appropriate amount of *N*-methyl-2-pyrrolidone (NMP, Aldrich). After intimate mixing and stirring, the resulting slurries were casted, respectively, on Al and Cu foils by doctor-blade technique. After drying at 70 °C to remove the NMP, disc electrodes (10 mm diameter) were punched and further dried at 110 °C under vacuum for 3 hours. Finally, the electrodes were stored in an argon-filled glove box with H_2O and O_2 contents lower than 1 ppm. Swagelok T-type sodium half-cells were assembled using 1 M $NaClO_4$ dissolved in either PC or PC : FEC (8 : 2 weight ratio). A glass fiber (Whatman) was used as separator. Sodium metal was cut from sodium pieces (Alfa Aesar), roll pressed and finally punched on the current collector. The $Na/Na_{0.6}Ni_{0.22}Fe_{0.11}Mn_{0.66}O_2$ cells were cycled galvanostatically at 15 mA g^{-1} within the 1.5–4.6 V range, while the Na/Sb–C cells were cycled within the 0.01–2 V range at different rates (10, 50, 100 mA g^{-1}). All the tests were performed at room temperature using a Maccor series 4000 battery tester (U.S.A). Cyclic voltammetry test was performed on the Na/Sb–C cell at a scan rate of 0.1 mV sec^{-1} within the 0.01–2.0 V *vs.* Na/Na^+ potential range at room temperature (25 °C) using a 1 M $NaClO_4$ in PC electrolyte, with a multi-channel potentiostat (VMP Biologic-Science Instruments).

The final full cell was assembled using 1 M $NaClO_4$ in PC-FEC electrolyte solution and galvanostatically cycled in the 4.1–0.7 V voltage range at 15 mA g^{-1} (respect to the cathode mass). Prior to full-cell assembly, the Sb–C anode was electrochemically activated by cycling it against a sodium metal electrode to eliminate the initial, irreversible capacity of the alloying material. Also, the electrode was loaded with Na ions to ensure a suitable negative-to-positive (N/P) capacity ratio for the proper cell balance.[30] The Sb–C to $Na_{0.6}Ni_{0.22}Fe_{0.11}Mn_{0.66}O_2$ mass ratio was of 0.75 (anode mass loading = 2.48 mg, cathode mass loading 3.3 mg). Considering a first charge capacity of 100 mA h g^{-1} for the pristine $Na_{0.6}Ni_{0.22}Fe_{0.11}Mn_{0.66}O_2$ electrode, and an average capacity of 180 mA h g^{-1} for the activated Sb–C electrode cycled at low rates (30 mA g^{-1}), the actual negative to positive (N/P) capacity ratio of the full cell was of about 1.3. All cells were assembled under inert conditions in an argon-filled glove-box.

References

1 D. Larcher and J.-M. Tarascon, *Nat. Chem.*, 2015, **7**, 19–29.
2 N.-S. Choi, Z. Chen, S. A. Freunberger, X. Ji, Y.-K. Sun, K. Amine, G. Yushin, L. F. Nazar, J. Cho and P. G. Bruce, *Angew. Chem., Int. Ed.*, 2012, **51**, 9994–10024.
3 M. Armand and J.-M. Tarascon, *Nature*, 2008, **451**, 652–657.
4 B. W. Jaskula, Lithium, in *Mineral Commodity Summaries 2012*, U. S. Geological Survey, Reston, VA, 2012, p. 94.
5 J.-M. Tarascon, *Nat. Chem.*, 2010, **2**, 510.
6 M. D. Slater, D. Kim, E. Lee and C. S. Johnson, *Adv. Funct. Mater.*, 2013, **23**, 947–958.
7 V. Palomares, P. Serras, I. Villaluenga, K. B. Hueso, J. Carretero-Gonzalez and T. Rojo, *Energy Environ. Sci.*, 2012, **5**, 5884–5901.
8 S.-W. Kim, D.-H. Seo, X. Ma, G. Ceder and K. Kang, *Adv. Energy Mater.*, 2012, **2**, 710–721.
9 N. Yabuuchi, K. Kubota, M. Dahbi and S. Komaba, *Chem. Rev.*, 2014, **114**, 11636–11682.
10 P. Moreau, D. Guyomard, J. Gaubicher and F. Boucher, *Chem. Mater.*, 2010, **22**, 4126–4128.

11 Y. Kawabe, N. Yabuuchi, M. Kajiyama, N. Fukuhara, T. Inamasu, R. Okuyama, I. Nakai and S. Komaba, *Electrochem. Commun.*, 2011, **13**, 1225–1228.
12 M. H. Hana, E. Gonzalo, G. Singh and T. Rojo, *Energy Environ. Sci.*, 2014, **8**, 81–102.
13 K. Kubota, N. Yabuuchi, H. Yoshida, M. Dahbi and S. Komaba, *MRS Bull.*, 2014, **39**, 416–422.
14 D. Buchholz, C. Vaalma, L. G. Chagas and S. Passerini, *J. Power Sources*, 2015, **282**, 581–585.
15 X. Wu, J. Guo, D. Wang, G. Zhong, M. J. McDonald and Y. Yang, *J. Power Sources*, 2015, **281**, 18–26.
16 I. Hasa, D. Buchholz, S. Passerini, B. Scrosati and J. Hassoun, *Adv. Energy Mater.*, 2014, **4**(15), DOI: 10.1002/aenm.201400083.
17 I. Hasa, D. Buchholz, S. Passerini and J. Hassoun, *ACS Appl. Mater. Interfaces*, 2015, **7**(9), 5206–5212.
18 B. L. Ellis and L. F. Nazar, *Curr. Opin. Solid State Mater. Sci.*, 2012, **16**(4), 168–177.
19 S. Komaba, W. Murata, T. Ishikawa, N. Yabuuchi, T. Ozeki, T. Nakayama, A. Ogata, K. Gotoh and K. Fujiwara, *Adv. Funct. Mater.*, 2011, **21**(20), 3859–3867.
20 Z. Du, R. A. Dunlap and M. N. Obrovac, *J. Alloys Compd.*, 2014, **617**, 271–276.
21 F. Klein, B. Jache, A. Bhide and P. Adelhelm, *Phys. Chem. Chem. Phys.*, 2013, **15**(38), 15876–15887.
22 V. L. Chevrier and G. Ceder, *J. Electrochem. Soc.*, 2011, **158**(9), A1011–A1014.
23 A. Darwiche, C. Marino, M. T. Sougrati, B. Fraisse, L. Stievano and L. Monconduit, *J. Am. Chem. Soc.*, 2012, **134**(51), 20805–20811.
24 B. Scrosati, J. Hassoun and Y.-K. Sun, *Energy Environ. Sci.*, 2011, **4**(9), 3287–3295.
25 W. X. Chen, J. Yang Lee and Z. Liu, *Carbon*, 2003, **41**(5), 959–966.
26 Y. N. Ko and Y. C. Kang, *Chem. Commun.*, 2014, **50**(82), 12322–12324.
27 M. He, K. Kravchyk, M. Walter and M. V. Kovalenko, *Nano Lett.*, 2014, **14**(3), 1255–1262.
28 L. Wu, X. Hu, J. Qian, F. Pei, F. Wu, R. Mao, X. Ai, H. Yang and Y. Cao, *Energy Environ. Sci.*, 2014, **7**(1), 323–328.
29 J. Qian, Y. Chen, L. Wu, Y. Cao, X. Ai and H. Yang, *Chem. Commun.*, 2012, **48**(56), 7070–7072.
30 S.-M. Oh, S.-T. Myung, M.-W. Jang, B. Scrosati, J. Hassoun and Y.-K. Sun, *Phys. Chem. Chem. Phys.*, 2013, **15**(11), 3827–3833.
31 J. Hassoun, G. Derrien, S. Panero and B. Scrosati, *J. Power Sources*, 2008, **183**, 339–343.
32 G. Derrien, J. Hassoun, S. Panero and B. Scrosati, *Adv. Mater.*, 2007, **19**(17), 2336–2340.